Conf-9311104--13

UCRL- JC-115684
PREPRINT

Two Dimensional Self-Consistent Fluid Simulation of RF Inductive Sources

Gregory J. DiPeso
Vahid Vahedi
Dennis W. Hewett
Thomas D. Rognlien

This paper was prepared for submittal to
AVS 40th National Symposium
Orlando, Florida
November 15 - 19, 1993

November 17, 1993

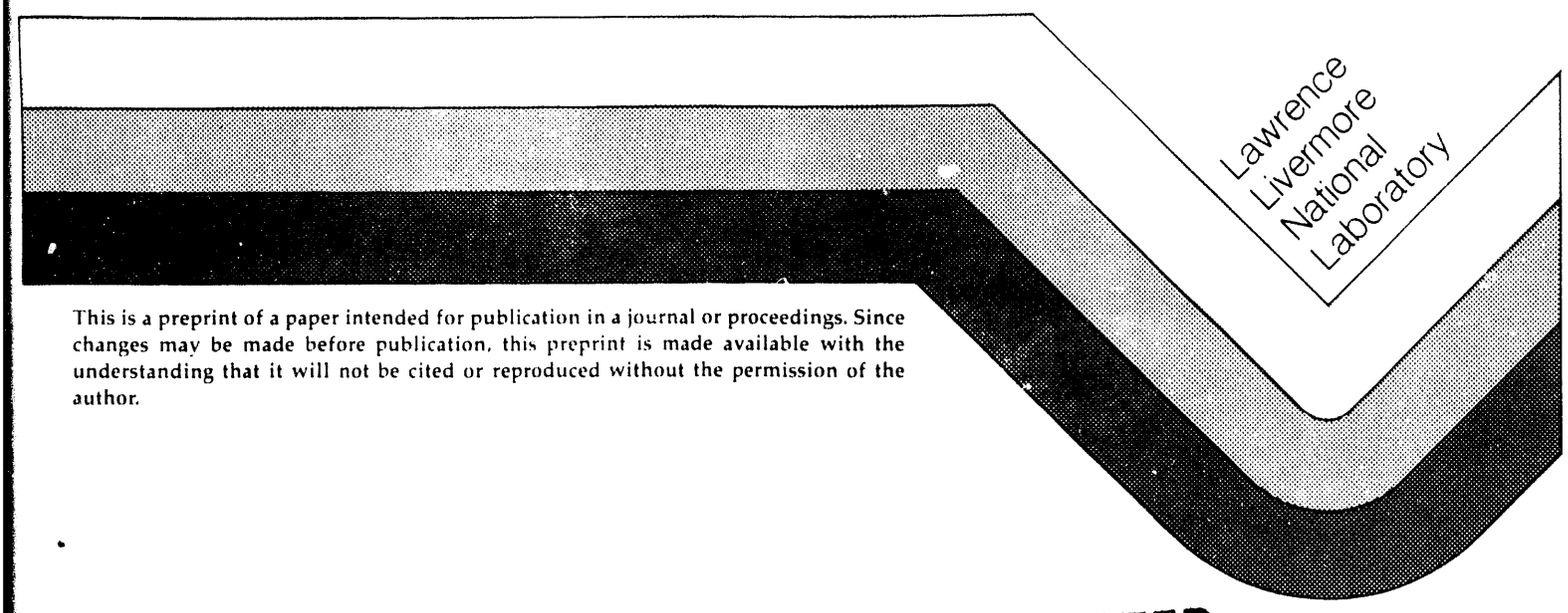

Two Dimensional Self-Consistent Fluid Simulation of RF Inductive Sources

G. DiPeso, V. Vahedi, D. W. Hewett, and T. D. Rognlien
Plasma Physics Research Institute and M Division
Lawrence Livermore National Laboratory
Livermore, CA 94550

November 4, 1993

Abstract

The two-dimensional $(R-Z)$ electromagnetic code FMRZ has been written to model inductive sources self-consistently in time. The code models an argon plasma with momentum-transfer, excitation and ionization as electron-neutral reactions and scattering and charge-exchange for the ion-neutral reactions. The electrons and ions are treated as Maxwellian fluid species and a reduced set of Maxwell's equations is used to advance the electromagnetic fields. The set of equations used in FMRZ is not subject to typical numerical constraints present in many time dynamic codes allowing one to choose appropriate time and space scales to resolve only the frequencies and scale lengths of interest. The model retains nonlinear driving terms which give rise to a pondermotive force that distorts the density profile. Density and power profiles will be used to illustrate the physical effects of various terms in the equations. Trends in average density and temperature compare well with an analytic model.

1 Introduction

Inductively coupled plasmas (ICPs) [1] [2] have been recently rediscovered as a plasma source for materials processing [3] [4]. Unlike the RF capacitive discharges currently used, ICPs can achieve higher plasma densities for increased throughput without a large sheath drop which can accelerate ions and cause workpiece damage. ICPs can also be run at lower pressures which leads to less collisionality and higher ion anisotropy for etching.

ICPs come in several geometric configurations. Simulation will help select the most effective

configuration for a given application by providing trends for changes in control variables such as neutral pressure, coil current, wafer voltage, etc. Figure 1 shows a typical ICP configuration and Fig. 2 shows our modeling geometry for the dielectric and flush coil cases. Our initial simulation efforts concentrate on the inductive coupling and so capacitive coupling on the coil side and the wafer side will be absent.

In contrast to many ICP simulations [5] [6], we simultaneously evolve the electromagnetic fields and the plasma response. We chose this approach partly based on our previous simulation experience with time dynamic codes. However, inclusion of time dynamics allows us to automatically keep nonlinearities such as the pondermotive force which distorts the density profile and can alter uniformity [7]. Futhermore, a time dynamic code is easily adapted to do particle-in-cell simulation to model electron kinetics.

We want only to resolve ω_{RF} and δ_{skin} to model power deposition and density profiles. Coevolving the full set of Maxwell's equations for the fields and fluid equations for the plasma requires the numerical resolution of small space scales, λ_{De}, and fast time scales, ω_{pe} and the light transit time across a numerical cell. For typical ICP parameters, $\omega_{pe} >> \omega_{RF}$ and $\lambda_{De} << \delta_{skin}$ and fast electromagnetic waves are not important to inductive coupling. To resolve RF, we need a numerical time step $\Delta t = 10^{-9}$ sec but if we had to resolve electron plasma oscillations, $\Delta t = 10^{-11}$ sec, and if we had to resolve light transit time across a typical numerical cell, $\Delta t = 10^{-13}$ sec.

A quasineutral Darwin model removes the unwanted scales by adding approximations to the first principal equations as opposed to damping the scales by implicit numerical methods. Quasineutrality removes the ω_{pe} and λ_{De} scales by avoiding charge separation. The Darwin or radiation free approximation removes the fast EM waves from Maxwell's equations by dropping the time derivative of the divergence free part of the electric field present in Ampere's Law. Quasineutral Darwin models have been used sucessfuly in pinch simulations and instability studies [8] [9] [10].

We started with the quasineutral Darwin code ZMR [9] which has been used to simulate theta pinches. ZMR uses axisymmetry to further simplify the field and plasma equations and the zero electron inertia approximation to remove electron cyclotron time scale which can also be numerically prohibitive in the presence of large external magnetic fields. It was pointed out, however, that without electron inertia at least in the θ component of the electron momentum equation, the external driving RF and the plasma current would always be in phase (or 180° out of phase), i.e., the resistive coupling would be present but the reactive coupling would be missing [11]. Since for our ICP parameters, $\omega_{RF} > \nu_{en}$, reactive coupling is important. Therefore, in addition to adding electron-neutral and ion-neutral collisions and modifying the ion fluid and electron temperature equations and boundary conditions, we added the θ component of the electron momentum equation that retains

inertia. For ICPs there is no strong external magnetic fields and so numerical resolution of the electron cyclotron time scale is not a concern. The overall reworking of the code prompted us to rename it FMRZ.

While FMRZ is still a fairly simple model, we have been able to use it to demonstrate pondermotive, coil placement, and ion-neutral collision effects on the plasma density profile. We have also compared FMRZ results with an analytic model and we have noticed similar trends in density versus power and density versus pressure.

The plan of this paper is as follows. In the second section, we will present our model and discuss its limitations. In the third section, we will show pondermotive, coil placement, and ion-neutral effects on the density profile and give some physical explanations for our observations. In the fourth section, we will show our comparisons with an analytic model. In the fifth section, some concluding remarks will be made.

2 The FMRZ Model

The model equations we are about to present are solved with simple finite forward time and centered space differencing. The only exceptions are a two-step predictor corrector advance for the electron θ momentum and an implicit Peaceman Rachford advance for the thermal conductivity term of the electron temperature equation.

The electron fluid equations are

$$n_e = n_i, \tag{1}$$

from quasineutrality,

$$u_{e\,r,z} = u_{i\,r,z}, \tag{2}$$

from r, z ambipolar diffusion, and

$$\begin{aligned} \partial_t n_e u_{e\theta} + [\nabla \cdot (n_e \mathbf{u}_e \mathbf{u}_e)]_\theta &= -e n_e E_\theta / m_e - e n_e [\mathbf{u}_e \times \mathbf{B}/(m_e c)]_\theta \\ &- [\nu_{ei} n_e (u_{e\theta} - u_{i\theta}) - \nu_{en} n_e u_{e\theta}], \end{aligned} \tag{3}$$

for electron θ momentum. Note that there is no pressure term because we retain ZMR's axisymmetry $\partial_\theta = 0$ assumption. We zero the derivative normal to the plasma edge for $u_{e\theta}$, i.e., $\partial_{\hat{\mathbf{n}}} u_{e\theta} = 0$ where $\hat{\mathbf{n}}$ signifies the unit vector normal to the edge. If this is only an approximation to the true boundary condition, it affects only the convective term of Eq. (3).

An energy balance gives the electron temperature equation

$$\partial_t T_e + \nabla \cdot (\mathbf{u}_e T_e) - \frac{T_e}{3} \nabla \cdot \mathbf{u}_e = \frac{2}{3 n_e} \nabla \cdot \kappa \nabla T_e - \frac{2 e^2}{m_e} n_e \eta_{ei} (T_e - T_i)$$

$$- \quad \nu_{iz}\epsilon_L + \frac{2e^2}{3} n_e[\eta_{ei}(u_{e\theta} - u_{i\theta})^2 + \eta_{en}u_{e\theta}^2], \tag{4}$$

where κ is a combine $e-n$ and $e-i$ thermal conductivity and the η terms are resistivity. The boundary condition is derived from an plasma edge energy flux balance between convection and conduction of energy into the sheath and an energy loss as the electron falls out of the sheath. The result is

$$\kappa \partial_{\hat{\mathbf{n}}} T_e + 5 u_B n_e T_e = 0, \tag{5}$$

where $u_B = (T_e/m_i)^{1/2}$.

For the ion advance, we use the usual set of fluid equations. The continuity equation is

$$\partial_t n_i + \nabla \cdot (n_i \mathbf{u}_i) = \nu_{iz} n_e, \tag{6}$$

The momentum equation is

$$\begin{aligned} \partial_t n_i \mathbf{u}_i + \nabla \cdot (n_i \mathbf{u}_i \mathbf{u}_i) &= -\nabla(n_i T_i/m_i) + e n_i \mathbf{E}/m_i + e n_i \mathbf{u}_i \times \mathbf{B}/(m_i c) \\ &- [n_i \nu_{ei}(\mathbf{u}_i - \mathbf{u}_e)(m_e/m_i) + n_i \nu_{in} \mathbf{u}_i], \end{aligned} \tag{7}$$

and in lieu of a proper energy equation we take

$$T_i = T_{neut}. \tag{8}$$

We apply our ion boundary conditions at the plasma sheath boundary which is $O(\lambda_{De})$ away from all walls since there is no driven electrode in these simulations. We pose physically reasonable boundary conditions without attempting to resolve λ_{De} sheaths. We take

$$\mathbf{u}_i \cdot \hat{\mathbf{n}} = u_B \tag{9}$$

and

$$\partial_{\hat{\mathbf{n}}}(\mathbf{u}_i \times \hat{\mathbf{n}}) = 0 \tag{10}$$

for the velocities and

$$- D_a \partial_{\hat{\mathbf{n}}} n_i = n_i u_B \tag{11}$$

for the density. The boundary conditions make the outflow flux equal the Bohm flux and is based on 1-D ambipolar diffusion theory where $D_a \approx T_e/(m_i \nu_{in})$.

We use the Darwin model and axisymmetry to simplify Maxwell's equations [12]. Starting with Ampere's Law

$$c\nabla \times \mathbf{B} = \partial_t \mathbf{E} + 4\pi \mathbf{J}, \tag{12}$$

the Darwin model drops the divergence free part of the displacement current to give

$$c\nabla \times \mathbf{B} = -\partial_t \nabla \phi + 4\pi \mathbf{J}. \tag{13}$$

Using axisymmetry, the θ component of Eq. (13) is

$$c(\partial_z B_r - \partial_r B_z) = 4\pi J_\theta. \tag{14}$$

Ambipolar diffusion and quasineutrality combine to allow no net current in the r and z directions. The divergence of Eq. (13) then gives $\nabla^2\phi = 0$ which is consistent with the quasineutral limit of Poisson's equation. Therefore, the remaining components of Eq. (13) give $B_\theta = 0$. Note that a B_θ in an ICP is yet to be measured [13].

The ∂_t of Eq. (14) can be combined with the r and z components of Faraday's Law to give

$$\partial_r \frac{1}{r}\partial_r r E_\theta + \partial_z^2 E_\theta = \frac{4\pi}{c^2}\partial_t J_\theta, \tag{15}$$

where the RHS can be formed from the sum of θ component momentum equations. Since electron momentum terms all dominate, we can multiply Eq. (3) by $-e$ and solve for $\partial_t J_{e\theta}$ and use this for the RHS of Eq. (15). An actual time differencing of $\partial_t J_\theta$ leads to a numerical instability [12]. With E_θ determined, we use the following equations for B_r and B_z:

$$\partial_t A_\theta = -cE_\theta, \tag{16}$$

$$B_r = -\partial_z A_\theta, \tag{17}$$

$$B_z = \frac{1}{r}\partial_r r A_\theta. \tag{18}$$

Equations (16)-(18) are restatements of the r and z components of Faraday's law that numerically assure $\nabla \cdot \mathbf{B} = 0$.

FMRZ solves Eqs. (15)-(18) for E_θ and $\mathbf{B}$ but E_r and E_z must be found. Although $\phi \approx 0$ giving no electrostatic (capactive) $\mathbf{E}$, $E_{r,z} \neq 0$ and can be calculated from the inertialess r and z components of the electron momentum equation which is appropriate to ambipolar diffusion. After substituting Eqs. (1) and (2) into the inertialess r and z components of the electron momentum equation and solving for the E_r and E_z, we get

$$E_r = -[\partial_r n_i T_e + e n_i u_{e\theta} B_z + m_e n_i \nu_{en} u_{ir}]/(e n_i), \tag{19}$$

$$E_z = -[\partial_z n_i T_e - e n_i u_{e\theta} B_r + m_e n_i \nu_{en} u_{iz}]/(e n_i). \tag{20}$$

Note the $u_{e\theta}$ terms in Eqs. (19) and (20). These terms contain a product of two quantities that are directly driven by the RF. These terms are therefore nonlinear and give rise to the pondermotive force. Equations (19) and (20) are used in the r and z components of Eq. (6) so that the force felt by the electrons is communicated to the ions thus affecting the density profile.

The boundary conditions for the electromagnetic fields are as follows. For $\mathbf{B}$, we enforce $\nabla \cdot \mathbf{B} = 0$ at all edges. No boundary conditions are required for E_r and E_z since they are determined by Eqs.

(19) and (20) and their gradients are never calculated. We use $E_\theta = 0$ at all conducting walls. At the coil side, we prescribe $E_\theta(r) = E_0 f(r)\cos(\omega_{RF}t)$ where $f(r)$ is a function chosen to model the coil and the dielectric window. For coils flush against the plasma as in Fig. 2, bottom, $f(r) = 1$ over the coil and $f(r) = 0$ where there is no coil. For a dielectric window between the plasma and the coil as in Fig. 2, top, we take a parabolic profile for $f(r)$ with a maximum of 1 and a minimum of 0. This is done to mimic the observed smoothing of the incoming field profile due to the dielectric window.

The amplitude E_0 is not fixed but adjusted at each RF cycle to insure that a given power is ohmically absorbed in the plasma. To see why this is so, consider a simplified version of Eqs. (4) and (6):

$$\dot{n} = \nu_{iz}n - u_B A n, \tag{21}$$

$$\dot{T}_e = \frac{P_{abs}}{Vn} - \nu_{iz}\epsilon_L, \tag{22}$$

where $n = n_e = n_i$ and A is the plasma surface area and V is the plasma volume. At equilibrium, the LHS of Eqs. (21) and (22) go to zero and we are left with a global particle balance that determines T_e and a global energy balance that determines n [14]. Now consider P_{abs}/V in terms of ohmic heating:

$$P_{abs}/V = \eta_{en}J_{e\theta}^2, \tag{23}$$

where $\eta_{en} = m_e\nu_{en}/e^2n$. Considering only the inertial and E_θ acceleration terms of Eq. (3) and assuming $E_\theta = E_0\exp(-z/\delta_{skin})\cos(\omega_{RF}t)$, the time average version of Eq. (23) becomes

$$P_{abs}/V = \frac{e^2\nu_{en}}{2m_e\omega_{RF}^2}E_0^2\exp(-2z/\delta_{skin})n. \tag{24}$$

Thus, to at least a linear approximation, P_{abs}/V is linear with n if E_0 is fixed. Substituting this linear form back into Eq. (22) removes the n dependence in that equations and so a system based on Eqs. (21) and (22) can never reach an equilibrium density. This problem becomes more apparent if the E_θ profile is less dependent on skin depth as is true for some two dimensionsal geometries in which a skin depth field solution is not valid.

That it is wrong to fix E_0 in a time dynamic code can be seen in a transformer coupled model of an ICP [15]. If the transformer secondary (plasma) properties are allowed to change, i.e. resistance and inductance changing in time, the electric field between the primary and secondary ($E_\theta(r)$) should be changing in time as well. We have sidestepped this problem by readjusting the amplitude so that a constant, chosen RF power is ohmically absorbed. After a few RF cycles, E_0 settles to a value which then drifts to an equilibrium value as the simulation approaches equilibrium. However, attempting to fix E_0 after equilibrium is acheived reintroduces the problem.

The limitations of the model are the E_θ and dielectric window and boundary condition modeling and more importantly the absence of collisionless heating and capacitive coupling. For our E_θ

inductive field equation, Eq. (15), the dielectric window can be modeled more accurately by attaching a region over which $\nabla^2 E_\theta = 0$ is solved. To calculate E_0, we can consider a transformer couple plasma model which gives the E_θ amplitude in terms of coil and plasma currents [15]. Collisionless heating can added to Eq. (4) if a accurate expression can be derived. A few authors have already made progress on this subject [16] [17]. It has been shown that the heating can be made to resemble an ohmic term and so for some fixed absorbed power, the additional heating mechanism reduces the calculated amplitude E_0.

Modeling capacitive coupling is essential to see how capacitive sheaths accelerate ions to etch the wafer or, unfortunately, the dielectric window. Capacitive coupling has been modeled by a drift diffusion approach [5] [6]. Equations (19) and (20) are solved for u_{er} and u_{ez} instead of E_r and E_z, Eq. (1) is replaced by an electron continuity equation similar to that of Eq. (6), and a Poisson equation is solved to determine E_r and E_z. The nonlinear terms in Eqs. (19) and (20) may or may not be included depending on how B_r, B_z, and $u_{e\theta}$ are determined. Substituting these equations in our model for quasineutrality and ambipolar diffusion approximations is quite possible. However, since proper modeling of inductive coupling required inclusion of electron inertia in the θ electron momentum equation, it seems reasonable to worry that proper modeling of capacitive coupled requires inclusion of electron inertia in the r and z electron momentum equations. Including these inertial terms while solving a Poisson equation reintroduces the ω_{pe} time scales which all interested parties would want to avoid.

If electron inertia is indeed needed for modeling of capacitive coupling, one way to avoid ω_{pe} time scales to solve the capacitive coupling equations for n_e, u_{er}, u_{ez}, and ϕ implicitly. Another approach would be to retain quasineutrality which is reasonable over the bulk of the discharge. A set of electron momentum equations similar to Eq. (7) could be solved and a quasineutral Poisson equation could be solved for ϕ and then E_r and E_z [18] [19]. The boundary condition for the quasineutral Poisson equation could be an analytic model for capacitive coupling. The boundary conditions Eqs. (5) and (9)-(11) would also have to be suitably modified.

3 Three Density Profile Effects

By turning off various terms in the equations or by altering boundary conditions, we can demonstrate many physical effects. Here, we have chosen to look at RF magnetic fields, flush coil placement, and constant diffusion. Our base case for comparision is an equilibrated $400W$, $5mTorr$ argon run with the geometry pictured in Fig. 2, top. All runs are said to equilibrate when the density at the mid-point is no longer changing in time.

The results of the base case run are shown in Fig. 3. Note the source or heating region extending about a skin depth away from the coil as shown on the ohmic heating plot. The resulting temperature profile is high on the source side but thermal conductivity exerts smoothing so that the temperature gradients are not extremely strong. The resulting ionization rate ν_{iz} which is temperature dependent also does not have strong gradients but would be high in the source region. The resulting density profile takes a diffusion shape. Note that the shape is not cosine/Bessel because of the asymmetry of the source region, the RF magnetic fields, and the non-constant diffusion from taking $\nu_{in} = [v^2_{th,\,ion} + v^2_{drift\,ion}]^{1/2}/\lambda_{mfp}$.

We first examine the importance RF magnetic fields by setting the fields to zero and comparing this run with the base case run. Figure 4 shows contour plots of the density with and without the RF magnetic field. The countour plots are oriented the same way as Fig. 2, top. Note that when the RF magnetic fields are kept, the density is pushed out of the source region and piles up causing a higher peak density value. The peak location itself shifts a little towards the source region, but the overall effect seems to push plasma away from the source region.

The effect can be explained via the pondermotive force [20] [7]. Consider the following electric field $E_\theta = E(z)\cos(\omega t + \phi)$. Faraday's law then gives a magnetic field of the form $B_r = (c/\omega)\partial_z E \sin(\omega t + \phi)$. Now consider a subset of the single particle equations of motion:

$$\dot{v_\theta} = (q/m)E_\theta, \tag{25}$$

$$\dot{v_z} = (q/m)v_\theta B_r/c. \tag{26}$$

Solving Eq. (25) for gives $v_\theta = (q/m\omega)E\sin(\omega t + \phi)$. Substituting this solution into Eq. (26), multiplying by m, and then taking the time average over an ω cycle gives the single particle force

$$f_z = -(q^2/4m\omega^2)\partial_z E^2. \tag{27}$$

Note that for any particle type and any phase ϕ the force is always opposite to the gradient in E_θ.

For ICPs with the coil at the top, the force pushes all particles out of the source region as we have observed in our simulations. The force is stronger for electrons than ions by a mass ratio. In fact, we noticed no observable difference from the base case when we set the RF magnetic field to zero for the ions only. It has been speculated that if the coils are placed on the sides, a centripetal force will cancel the pondermotive force thus keeping particles in the source region where they can be heated more efficiently [21].

We next examined the effect of placing the coils flush with the plasma. This is analagous to having so much current in the coil that the dielectric window cannot smooth the incoming field. Figure 5 shows the same group of plots a Fig. 3. Notice that the temperature and density profiles are essentially the same except the coil shape starts to penetrate into the plasma. For a shorter

device or higher powers, the coil shape could penetrate through the entire plasma so that the coil image could be etched onto the wafer. Also notice that the density peak is slightly higher for the flush coil case. This may correspond to the E_θ amplitude also being larger which leads to a stronger pondermotive force.

Finally, we looked at constant diffusion by calculating $\nu_{in} = v_{th\,ion}/\lambda_{mfp}$. This form of ν_{in} makes the ambipolar diffusion coefficient a constant so that one can proceed with a two dimensional analytic calculation of the density profile [22]. This form would be accurate if ion drift velocities were much smaller than ion thermal velocities, but for ICPs this is seldom the case. Changing to this form of ν_{in} in the simulation is trivial and the effect is observed in Fig. 6. Note that the density profile in the non-constant diffusion is flatter along z but with a sharp drop at the ends where as the density profile in the constant diffusion case is much more peaked in z.

The effect can be explained in terms of diffusion theory. At the edge of the plasma, we have Bohm flux outflow, which by Fick's law is equal to the product of the diffusion coefficent and the density gradient. When nu_{in} is calculated with the ion drift velocity instead of the of the ion thermal velocity, the diffusion coefficient is smaller, and for the same Bohm flux outflow, the density gradient must be larger. Since our code borrows from diffusion theory, it should be no suprise that diffusion theory arguments work well. However, as this section has demonstrated, the profile can be strongly affected by geometry and nonlinear effects as well.

This diffusion effect has also been observed by Godyak in his one dimensional analytic calculations [23]. We are attempting to extend our analytic method to capture this effect in two dimensions. The inclusion of ion drift velocity in the ambipolar diffusion coefficient makes the diffusion equation nonlinear and so a simple closed for in two dimensions is elusive.

4 Comparision with an Analytic Model

We compared our simulation with an analytic model derived from diffusion theory [22]. The analytic model gives a cosine/Bessel profile for the density. The simulation contains other effects besides diffusion, such as the pondermotive force, source region asymmetry, and convection in the fluid equations. To make comparisons, we ran our simulation with $\nu_{in} = v_{th\,ion}/\lambda_{mfp}$.

Figure 7 shows that while absolute values of average n and T_e do not match, the linear trend of average n with absorbed power and the independence of average T_e with power is observed for both the simulation and the analytic model. Furthermore, both analytic model and simulation give increasing density and decreasing temperature with increasing neutral pressure. Note similar trends are also observed experimentally [21] [24].

5 Conclusion

In this paper, we have described our time dynamic code for the simulation of ICPs and have shown that with the nonlinear terms in the fluid equations automatically retained, the pondermotive force effect on the density profile can be easily observed. We have also presented coil placement and correct ν_{in} effects on the density profile and checked the code's global response with an analytic theory.

While a time dynamic code that follows ω_{RF} requires more computer time to reach steady state than a code that assumes an $e^{j\omega_{RF}t}$ variation on driven quantities, we believe that the physics retained and the flexibilty to add more physics is worth the effort. Quick answers and trends can already be supplied by analytic models where as simulations can be used to deepen understanding and support analytic models.

Acknowledgements

We wish to thank Prof. Mike Lieberman for many useful discussions about inductively coupled plasmas and for his helpful insight into both our simulation and analytic models.

Work performed under the auspices of the United States Department of Energy by the Lawrence Livermore National Laboratory under contract number W-7405-ENG-48.

References

[1] W. Hittorf, *Wiedemanns Ann. d. Physik* **21**, 90 (1884).

[2] H. U. Eckert, *Proc. 2nd Intl. Conf. on Plasma Chem. and Technol.*, H. Boenig, ed., Technomic Publ., Lancaster PA (1986).

[3] J. H. Keller, M. S. Barnes, and J. C. Forster, Abstract NA-5, 43rd Annual Gaseous Electronics Conference, Urbana-Champaign, IL, October 16-19, 1990.

[4] Lam Research Corporation, Technical Note TN-003 (1992).

[5] P. L. G. Ventzek, R. J. Hoekstra, T. J. Sommerer, and M. J. Kushner, *Appl. Phys. Lett.* **63**, 605 (1993).

[6] R. A. Stewart, P. Vitello, D. B. Graves, AVS Topical Conference: The 2nd Workshop on High Density Plasmas and Applications, San Francisco, CA, August 5-6, 1993.

[7] J. C. Helmer and J. Feinstein, AVS Topical Conference: The 2nd Workshop on High Density Plasmas and Applications, San Francisco, CA, August 5-6, 1993.

[8] J. A. Byers, B. I. Cohen, W. C. Condit, and J. D. Hanson, *J. Comput. Phys* **27**, 476 (1978).

[9] D. W. Hewett, *J. Comput. Phys.* **38**, 378 (1980).

[10] D. S. Harned, *J. Comput. Phys.* **47**, 452 (1982).

[11] M. A. Lieberman, Private Communication, (1993).

[12] C. W. Nielson and H. R. Lewis, in *Methods in Computational Physics*, Vol. 16, p. 367, edited by B. Alder, S. Fernbach, M. Rotenberg, and J. Killeen (Academic Press, New York, 1976).

[13] J. Hopwood, C. R. Guarnieri, S. J. Whitehair, and J. J. Cuomo, *J. Vac. Sci. Technol. A* **11(1)**, 147 (1993).

[14] M. A. Lieberman and R. A. Gottscho, Electronics Research Laboratory, Memo UCB/ERL M93/3 (1993).

[15] J. W. Denneman, *J. Phys. D: Appl. Phys.* **23**, 293 (1990).

[16] M. M. Turner, *Phys. Rev. Lett.* **71**, 1844 (1993).

[17] V. Godyak, 46th Annual Gaseous Electronics Conference, Montreal, Quebec, Canada, October 19-22, 1993.

[18] D. W. Hewett and C. W. Nielson, *J. Comput. Phys.* **29**, 219 (1978).

[19] G. DiPeso, D. W. Hewett, and G. F. Simonson, *accepted for publication, J. Comput. Phys.* (1993).

[20] F. F. Chen, *Plasma Physics and Controlled Fusion*, Vol. 1, (Plenum Press, New York, 1984).

[21] L. J. Mahoney, C. J. Richards, A. E. Wendt, and J. L. Shohet, AVS Topical Conference: The 2nd Workshop on High Density Plasmas and Applications, San Francisco, CA, August 5-6, 1993.

[22] V. Vahedi, G. DiPeso, D. W. Hewett, and T. D. Rognlien, *submitted to J. Vac. Sci. and Technol.* (1993).

[23] V. Godyak, *Soviet Radio Frequency Discharge Results*, (Delphic Associates, Inc., Falls Church, VA, 1986).

[24] J. Hopwood, C. R. Guarnieri, S. J. Whitehair, and J. J. Cuomo, *J. Vac. Sci. Technol. A* **11(1)**, 152 (1993).

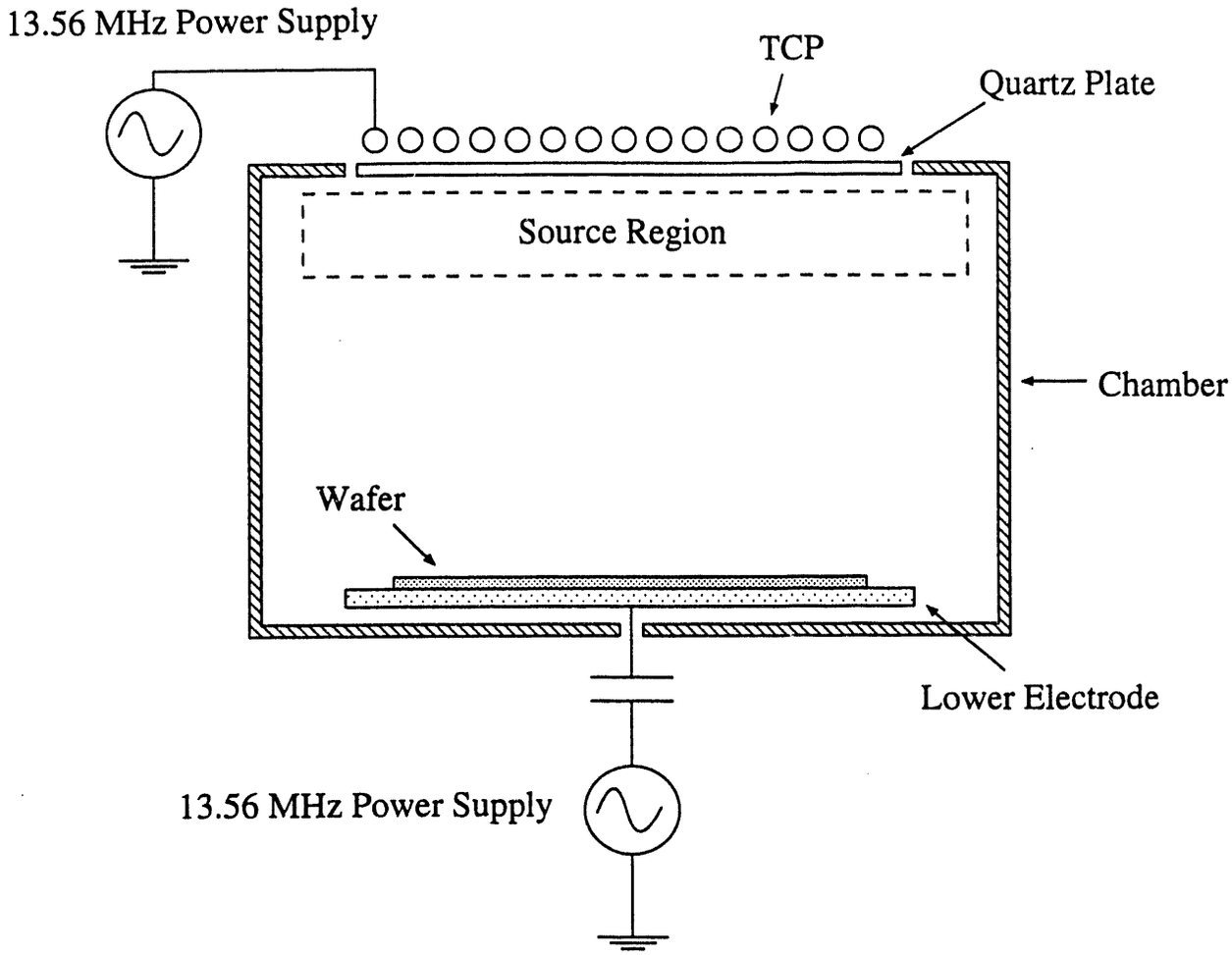

Figure 1: An ICP reactor. Typical parameter ranges are:

Plasma Density $10^{10} - 10^{12}/cm^3$

Neutral Pressure 1 – 50 mTorr

Power Absorbed 100 – 5000 W

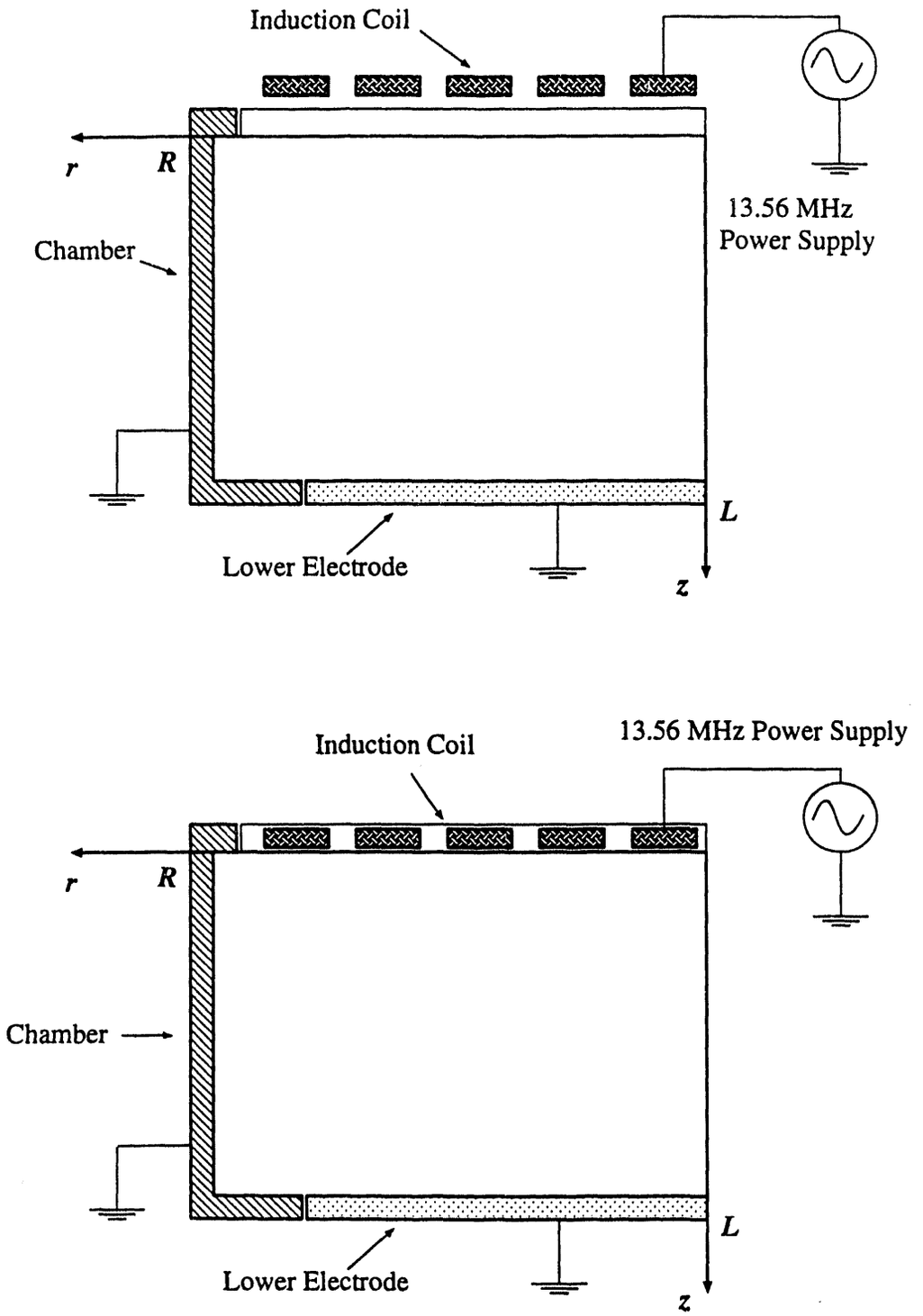

Figure 2: The top figure shows our normal modeling geometry and the bottom figure shows our modeling geometry for coils flush with the plasma.

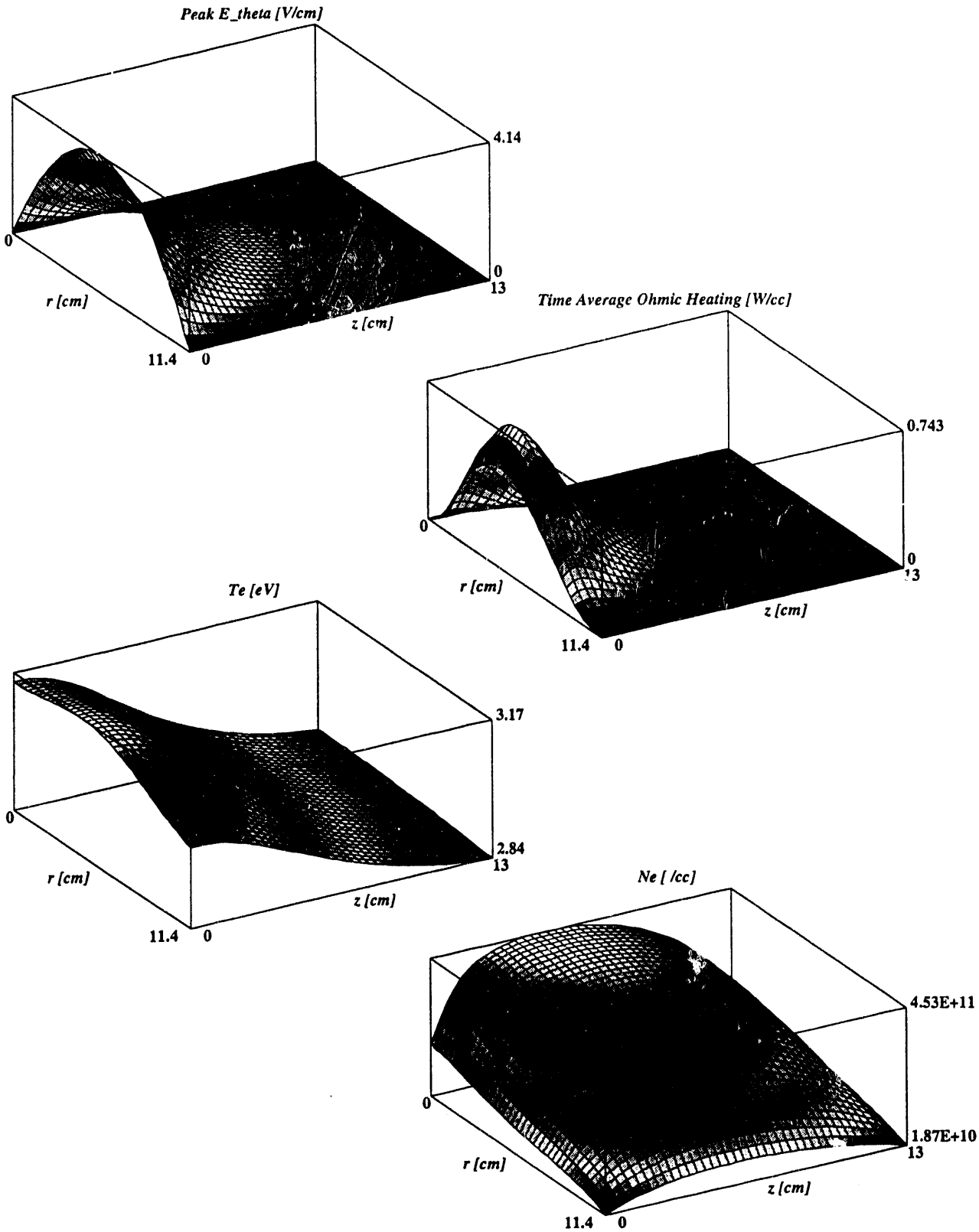

Figure 3: Base case simulation at 400W, 5mTorr. T_{neut} =300K, R = 11.4 cm, Z=13cm, and ω_{RF} = 13.56MHz.

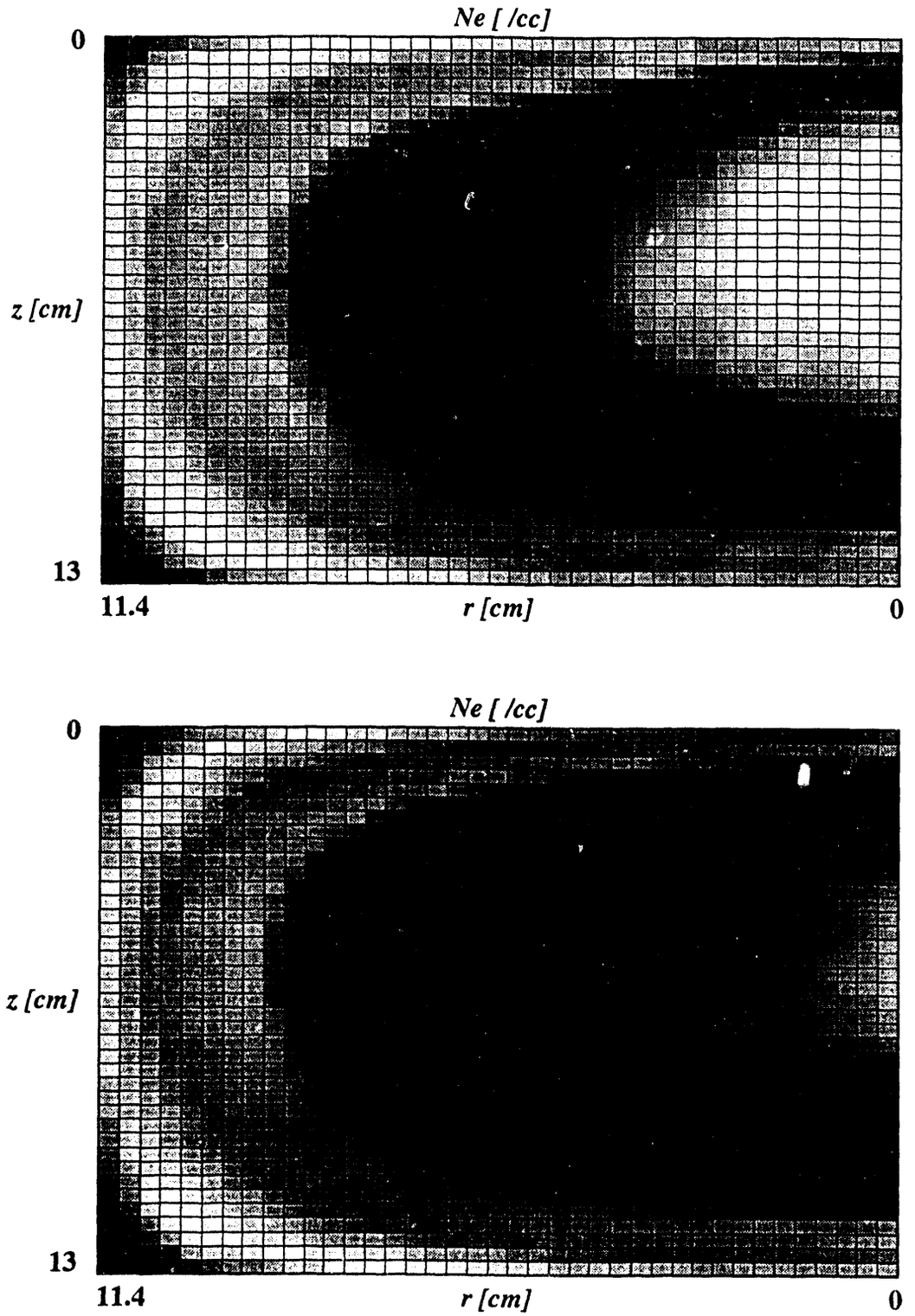

Figure 4: The top figure shows density contour with $\mathbf{B}_{RF} \neq 0$. The peak density is 4.53×10^{11} /cc. The bottom figure shows density contour with $\mathbf{B}_{RF} = 0$. The peak density is 4.19×10^{11} /cc. Both contours were drawn over the range 1.8×10^{10} /cc to 4.6×10^{11} /cc for comparison.

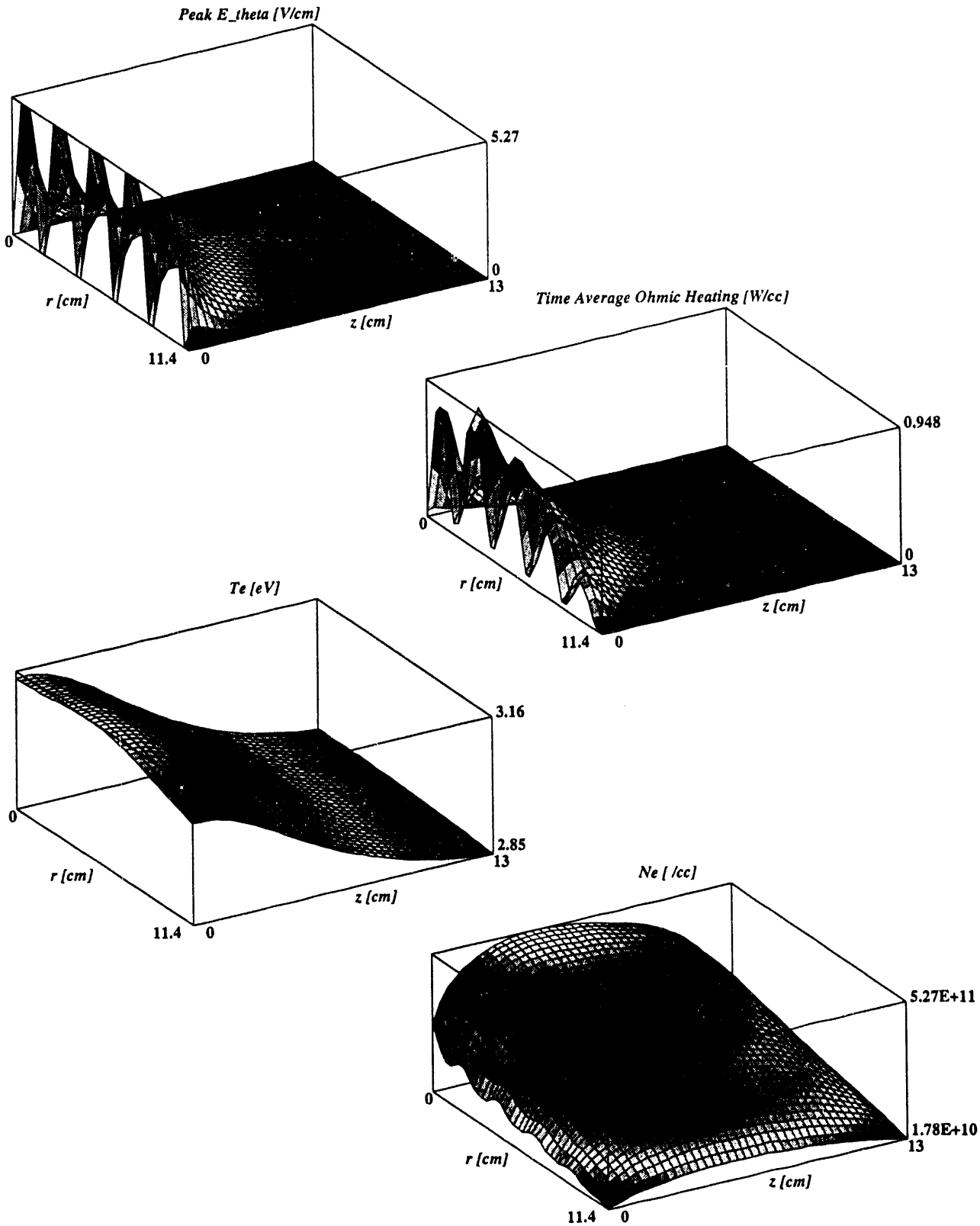

Figure 5: Parameters are the same as the base case simulation except the coil are flush with the plasma.

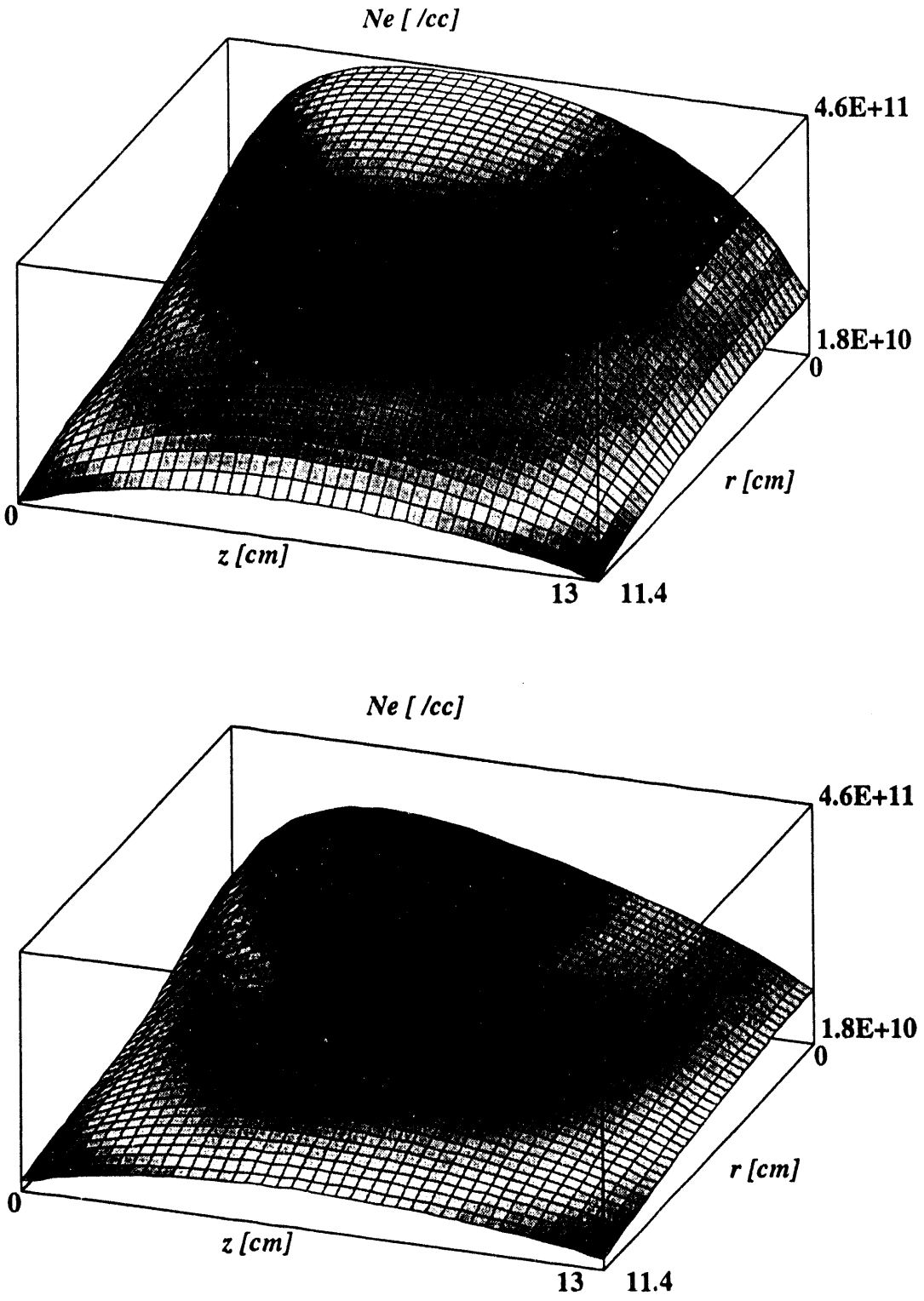

Figure 6: The top figure shows the density profile with $\nu_{in} = [v^2_{th\,ion} + v^2_{drift\,ion}]^{1/2}/\lambda_{mfp}$. The density range along z at $r = 0$ for this case is 1.21×10^{11} /cc to 4.53×10^{11} /cc. The bottom figure shows the density profile for the constant diffusion case in which $\nu_{in} = v_{th\,ion}/\lambda_{mfp}$. The density range along z at $r = 0$ for this case is 1.12×10^{11} /cc to 3.41×10^{11} /cc.

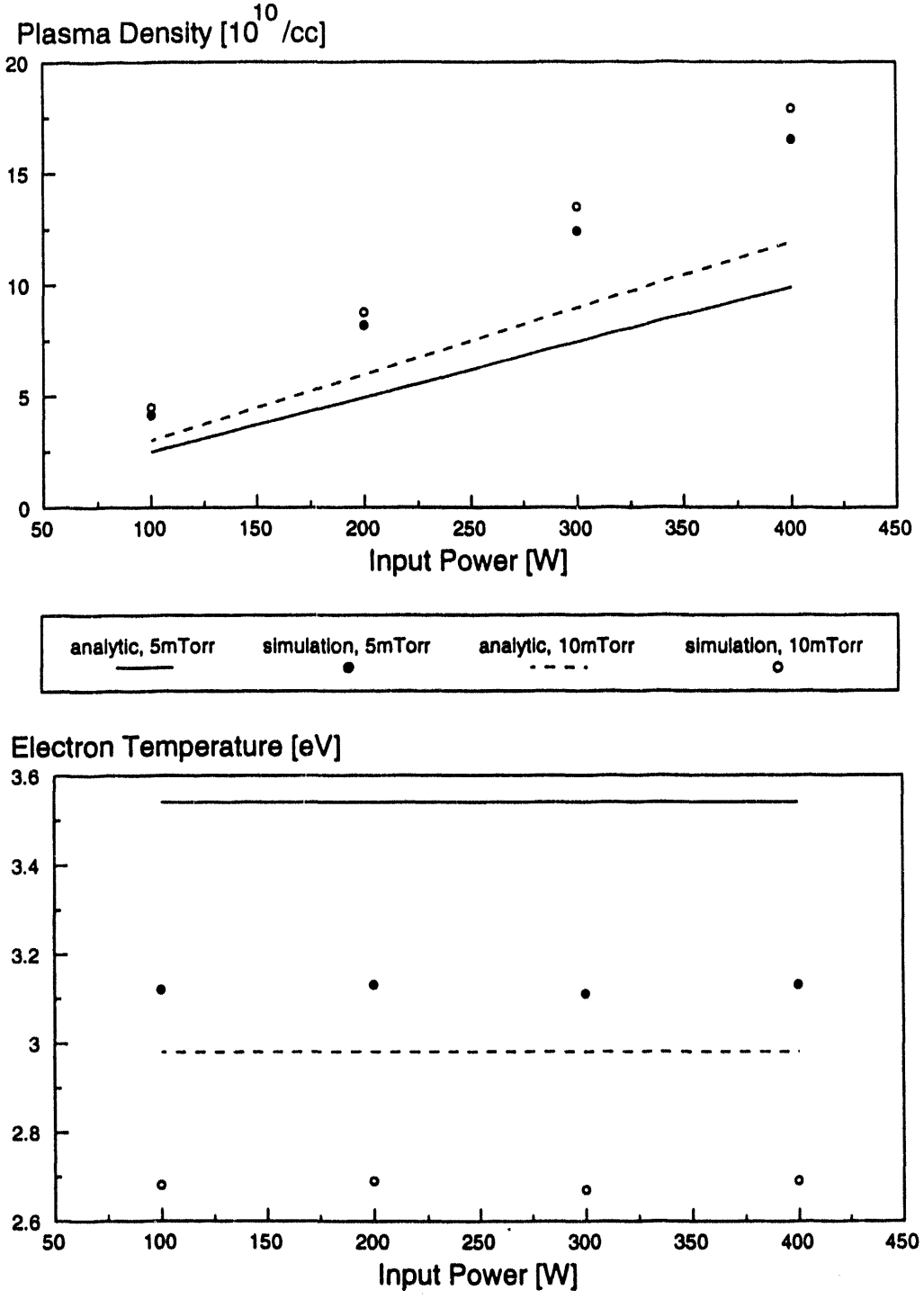

Figure 7: Comparison of average density and temperature calculated by simulation and an analytic model. The system parameters are the same as shown on Fig. 3.

END

DATE FILMED

1/12/94